

DESIGN AND RELIABILITY OF CERAMICS:
DO MODELERS, DESIGNERS, AND
FRACTOGRAPHERS SEE THE SAME WORLD?

Ceramic Engineering and Science
Proceedings,
Vol. 26, [8] pp. 239 - 252 (2005).

George David Quinn
National Institute of Standards and Technology
100 Bureau Drive
Gaithersburg, MD, 20899-8529

ABSTRACT

Techniques for design and reliability analyses of structural ceramic components are now well established. Laboratory test coupon data are used in design codes to predict the fast fracture and time dependent reliability of monolithic or dispersed-phase ceramic composite components. Fractographic analysis of fractured components shows that there can be surprises, however. A few case studies are reviewed to show that components often fail from an unanticipated cause. The reliability models make a number of assumptions that, if violated, put the predictions at risk.

INTRODUCTION

The general design concepts for reliability analysis of monolithic structural ceramics have been by now well established. These are not recapitulated in detail here and the reader is referred to any one of a number of good reviews. [1,2,3,4,5,6,7,8,9] Referring to Figure 1, the ceramic component is envisioned as having volume, surface and/or edge type strength limiting flaws. Which of these cause fracture depends upon the stress state in the part. So for example, a component loaded in uniform tension is more apt to trigger failure from the largest flaw than if the component were loaded in bending. Weibull analyses have long been used successfully to model the probability of fracture or survival [1]. Complex structures may be analyzed by finite element models and the stress distributions fed to other programs that integrate the risk of rupture over all elements in the body. Time-dependent reliability is customarily analyzed by modeling subcritical flaw growth that can weaken the component, until one flaw reaches criticality leading to component fracture. If the component is exposed to elevated temperature, then temperature dependent properties and crack growth behavior must be factored in.

Although this is the conventional analysis for mechanical reliability of structural ceramics exposed to tensile stresses, it should be kept in mind that other failure mechanisms such as wear, erosion, creep fracture, or compression fracture can also cause "failure" or loss of function.

Despite the widespread acceptance of this general approach, there are considerable variations in the details, and indeed, the devil may be in the details. What is the best Weibull analysis to use? Should a two parameter or three parameter distribution be assumed? What is the best way to estimate the distribution parameters? Are they biased? How much laboratory data should be collected? What type of lab data? Is stress rupture data better than

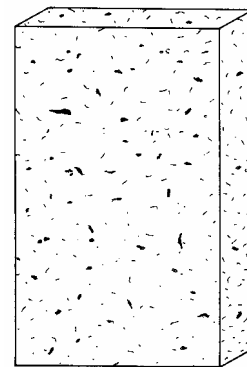


Figure 1 A ceramic component with a myriad of flaws.

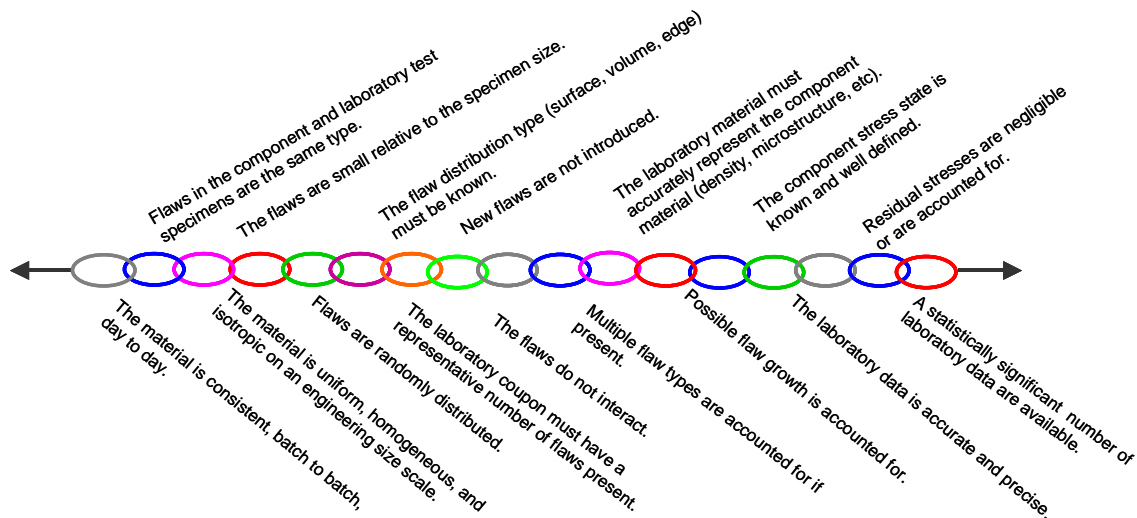


Figure 2 The weakest links in a design and reliability model may be the model assumptions.

dynamic fatigue or crack velocity data? Is there a threshold stress or stress intensity below which crack growth will not occur? What is the best multiaxial stress failure criterion? Should one use test data based on indentation flaws or genuine material flaws? What are the uncertainties and errors? How far, if at all, may one extrapolate?

One finds that the record is rather mixed for hundreds of ceramic reliability and design analyses. There have been some spectacular successes and many failures. This prompted Morrell in 1989 to question the value of any laboratory test coupon data for reliability analysis, and to suggest that component testing is a sounder approach.[10] A review by Quinn and Morrell [11] in 1991 investigated this matter in more detail, principally in the context of whether flexural strength test data had value for design. They concluded that the general design concepts for reliability analysis were sound, but that the analyses make a series of critical assumptions about the material, the flaws, and the nature of the loading. Only if all the assumptions were valid, could one expect the reliability models to be accurate. Otherwise, the models could make very erroneous predictions. Indeed, the whole affair may be likened to weakest link theory as shown in Figure 2, except that in this instance the links are the model assumptions. The final conclusion in the review was that laboratory scale flexural strength data could be used for design, but one had to be lucky. By this it was meant that more often than not nature violates one or more of the assumptions. This sobering conclusion should not be limited to flexure strength data either: any reliability analysis based on any laboratory coupon data has the same risks. Quinn and Morrell recommended that test coupons of different sizes be tested to search for multiple flaw types and to validate the size-scaling model. Ideally, specimens should be cut from the component to compare to the separate laboratory coupon data sets. They summarized: “The reliability of any design extrapolation is likely to be best when the test bar most closely related to the component in terms of size, stress state, and defect distribution.”

One might wonder that if there were so many caveats, whether any design with brittle ceramics has ever succeeded. The record shows that indeed there are a number of successful cases, often because the investigators paid close attention to the assumptions in Figure 2 [11].

This paper gives four case studies wherein fractographic analysis revealed critical information that should be included in a reliability model. The primary point of this paper is that

judicious use of fractographic analysis of laboratory strength coupons and destructive prototype testing can dramatically improve reliability models and databases.

CASE 1 The Ford Gas Turbine Rotor

This was an ambitious but well thought out small project conducted at the Ford Motor Company's Scientific Research Laboratory^a in the late 1970's to mid 1980's.[12,13] It was part of a much larger endeavor to incorporate advanced ceramics into automotive gas turbine engines. Considerable effort was expended on improving ceramic materials, developing reliability codes, generating data bases, fabricating parts, and running them in test rigs. Full scale engine testing was extremely expensive and risky, so it was decided that a small project would be performed to verify the ceramic design and reliability codes by using a realistic model component shown in Figure 3. This simulated gas turbine rotor was mounted in a hot spin rig shown in Figure 4 and rotated at 50,000 rpm while heated by hot gasses to a peak rim temperature of 1260 °C (2300 °F).

Ten model rotors were fabricated and tested. The component was designed to have a high probability of survival on loading (> 95 %), but to probably fail within 25 h. The design analysis was based on the premise that failure would occur due to slow crack growth of preexisting flaws that were distributed throughout the volume. It was expected that fracture would occur from the thin web portion of the rotor where the stress and temperature were both high. The intent was to compare the actual rotor lifetimes to predictions from the reliability codes, refine the models as needed, and identify the best type of laboratory test data.

The model rotor was made of a state of the art hot-pressed silicon nitride^b (NC 132) that was carefully machined to final dimensions. The particular grade was one of the most thoroughly analyzed structural ceramics of all time and was eventually used as the world's first reference material for the property fracture toughness.[14] Eventually enough data was available that a comprehensive fracture mechanism map was constructed,[15] but that was after the



Figure 3 Ford silicon nitride model gas turbine rotor #1323 which survived 25 h intact. The model rotor has a 95 mm diameter.

^a Certain commercial materials or equipment are identified in this paper to specify adequately the experimental procedure. Such identification does not imply endorsement by the National Institute of Standards and Technology nor does it imply that these materials or equipment are necessarily the best for the purpose.

^b Grade NC 132, Norton Co., Worcester Ma.

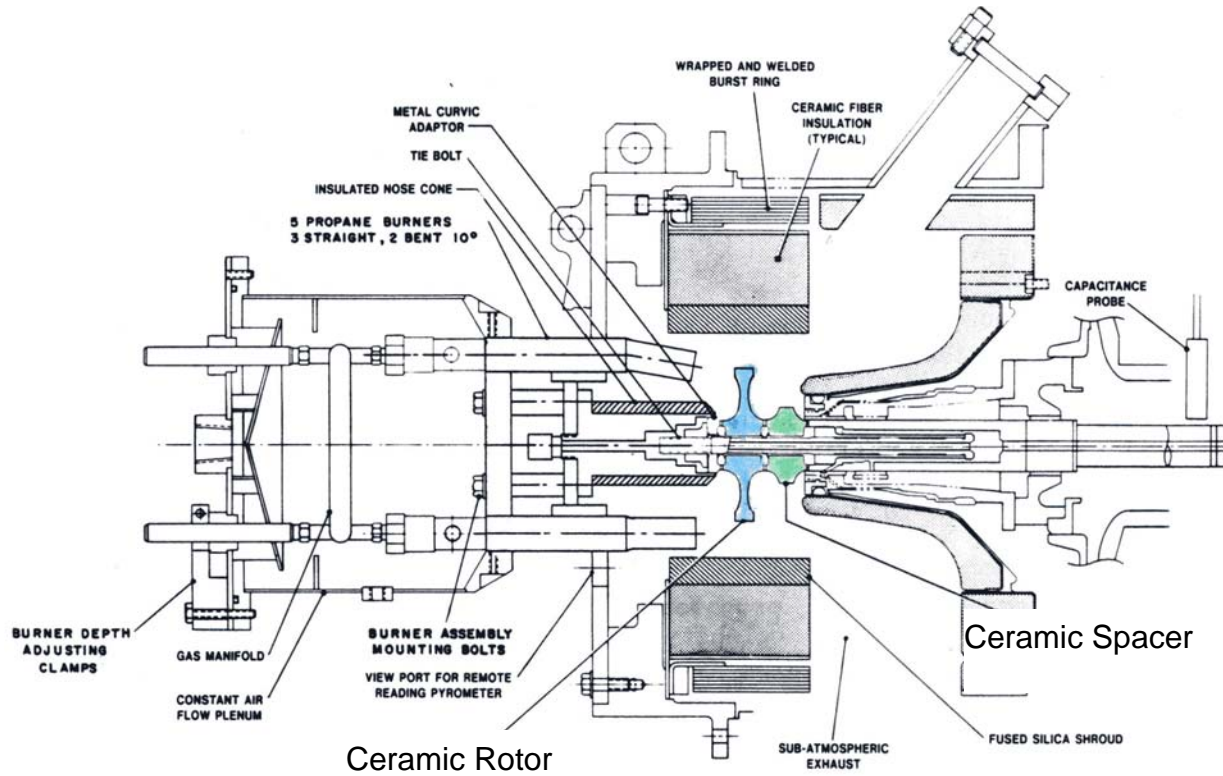


Figure 4 The Ford hot spin test rig (Figure from Ref. 12).

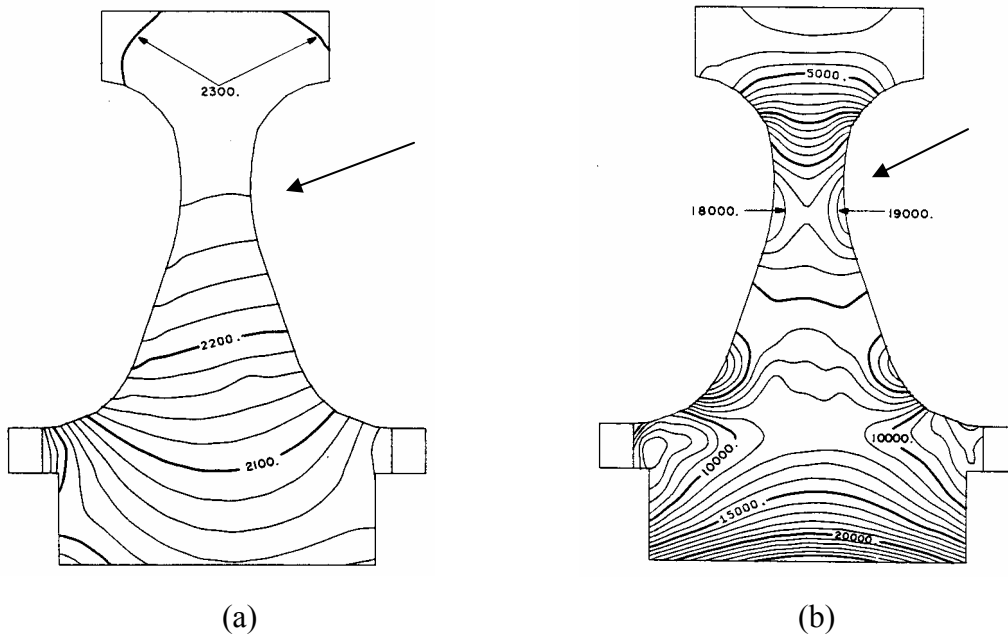


Figure 5 Isotherms ($^{\circ}\text{F}$) (a), and maximum principal stresses (psi) (b) in the rotor. Failure was expected to occur in the thin web (large arrows) (Figures from Ref. 12). The maximum stress in the web was oriented primarily in a radial direction.

conclusion of the Ford rotor test project. A substantial amount of laboratory test coupon data were available including flexural and tensile strengths, elastic properties, and slow crack growth parameters. All were available as a function of temperature. Slow crack growth data were available from three types of tests: variable stressing rate strength tests (dynamic fatigue), crack velocity - fracture mechanics tests (double torsion), and stress rupture (flexural and tensile). The model rotor did not have turbine vanes, but an increased rim mass to simulate their effect. Figure 5 shows the temperature and principal stresses from the heat transfer and finite element models, respectively. The maximum principal steady state stress was 131 MPa (19,000 psi).

Figure 6 shows the reliability as a function of time. An estimate of the error in the calculated reliabilities was made using estimated temperature errors of $\pm 11\text{ }^{\circ}\text{C}$ ($20\text{ }^{\circ}\text{F}$). At time zero, the reliability was simply the fast fracture reliability that was evaluated by integrating the normal stress around the unit sphere in each element and evaluating the Weibull volume integral for each element. The three types of slow crack growth data gave very divergent predictions. Figure 6b shows the outcomes for the six rotors that failed at times from 0.2 h to 18.6 h. Three other rotors survived 24 h and a fourth at 13 h and were treated as censored outcomes (not shown). The predictions made with the stress rupture data set gave the best correlation to the actual lifetimes and the authors concluded that stress rupture data is the best for predicting reliability versus time.[12] This outcome was gratifying to this author since his data were used for the predictions.[16]

So in this case, the designer and modeler saw a ceramic component designed to fail from slow crack growth of preexisting volume flaws located in the rotor web. What did the fractographer see?

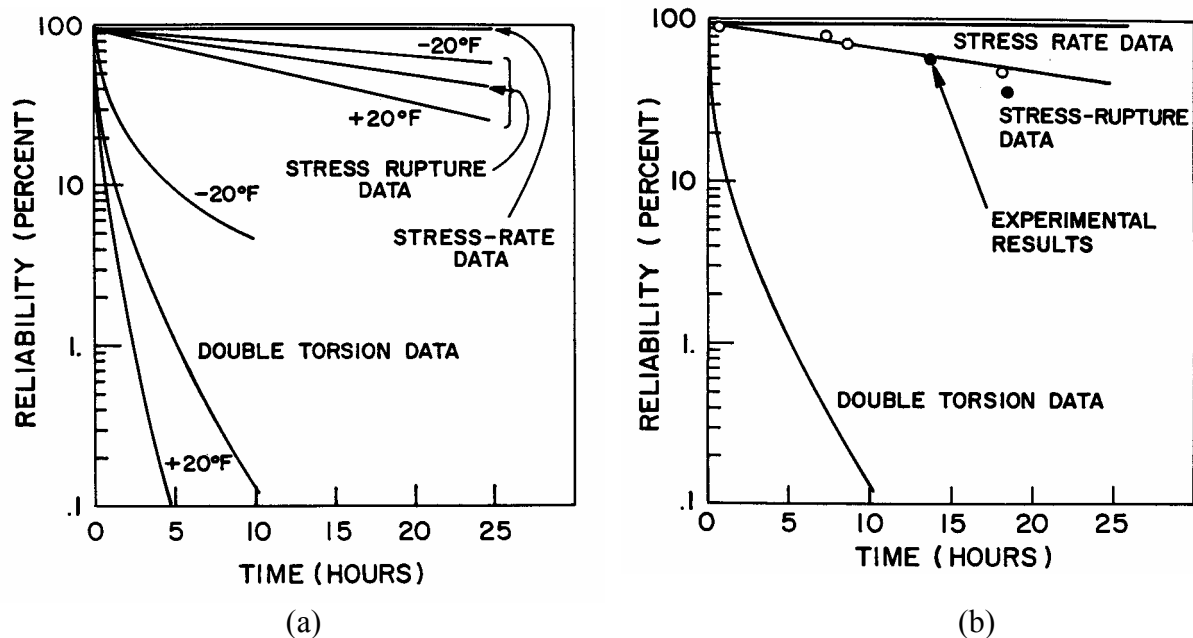


Figure 6 Reliability versus time. (a) shows the predictions and estimated uncertainty limits for expected temperature variations, and (b) shows the actual outcomes for six rotors that failed while running hot at 50,000 rpm (Figures from Refs. 12, 13). The two solid points are the rotors that were fractographically analyzed by the author.

The fractographic analysis revealed that fracture did not occur quite as anticipated. The test rig was constructed in such a manner that most broken fragments were retrievable. The longest (18.6 h) and third longest (13.8 h) rotors were sent to the author for fractographic evaluation. It was felt that these would have large slow crack growth zones that would be easy to find. One virtue of NC 132 is that it was a very fine-grained fully dense material with minimal second phase. Fracture markings were quite clear and the local direction of crack propagation could be assessed in every piece. Rotor # 1324 (18.6 h) was reconstructed piece by piece over the course of one week culminating in the assembly shown in Figure 7. Many fragments from the rim were missing, but it did not matter. The figure also shows that the spacer had also fractured and its pieces were commingled with the rotor thereby hampering the assembly. Nevertheless, the central portion and web portion of the rotor was almost completely reassembled. After completion, the rotor was taken apart again and a map of crack propagation directions was made.

The interpretation was clear. Primary fracture commenced at the bore or the curvic coupling teeth and cracks branched and ran out to the rim as shown in the Figure 7 schematic. Every single fragment was examined in a futile search for a web origin and/or slow crack growth zone, but none were found. All primary fractures started from the bore or coupling area. There were three origins from the inner part of the rotor. Origin "A" was in the bore at the exact edge of the bore, which although chamfered nonetheless had surface grinding cracks (Figure 8). It could not be determined whether slow crack growth had enlarged the grinding cracks. The other two origins were located on the other side of the bore and were from the curvic coupling teeth machined into the rotor. These were part of the attachment scheme. One origin was a transverse machining crack and the other was an impact – contact crack.

Thus, fracture started on one side of the rotor, thereby opening up the disk structure whereupon unbalanced forces triggered a rupture on the opposite side. Origin A had a well-defined small fracture mirror allowing an stress estimate of a 630 MPa (92 ksi) which is much greater than the model estimated bore stress of ≈ 172 MPa (25 ksi) from Figure 5. This, plus the violent branching from site A, suggest it was a secondary fracture. Primary fracture occurred on the other side of the bore, causing the rotor to go completely out of balance leading to the overstress fracture at point A. Origin h was a large contact crack flaw with a very large mirror. The local stress was estimated to be 500 MPa (72 ksi) from the flaw size and approximately 580 MPa (84 ksi) from the fracture mirror. Origin g was determined to have fractured after site h. Figure 5 shows there were modest bore stresses (≈ 138 MPa, 20 ksi) and temperatures (1150 °C, 2200 °F), but the stress does not match the level assessed by fractographic analysis.

One other possibility is suggested by an observation from the fractographic examination. When the rotor and spacer were assembled in the hot test rig, it was customary to separate them with a thin platinum foil to prevent direct ceramic-to-ceramic contact. The fractographic examination showed uneven platinum wear traces and even some bare spots. Could it be that the foil deformed or crept with time such that ceramic-to-ceramic contact eventually occurred? If so, then the rotor stress distribution may have become unbalanced or local stress concentrations or contact stresses may have contributed to cause initial fracture at site h.

This exercise was a good example of one of the author's laws of fractography: "The first one is the hardest." While at first glance reassembly of an exploded rotor may appear to be a formidable task, it was merely time consuming. The second rotor, #1314, took less time to analyze. It also had fracture initiation sites at the bore or at the teeth. Years later, the author became aware of comparable work done on model silicon nitride rotors at Daimler-Benz.[17] They also reconstructed burst silicon nitride rotors and used fractography to find that grinding cracks in the bores sometimes were fracture origins.

Some lessons learned from our fractographic analyses were:

- Fracture occurred from a different cause than expected and modeled.
- Stress rupture data may have been the best for reliability estimation, but the correlation of failure times was fortuitous for the two rotors examined.
- Volume flaws were not found in the two fractured rotors. Surface machining cracks were found and thus, Weibull area scaling should also have been included in the reliability model.

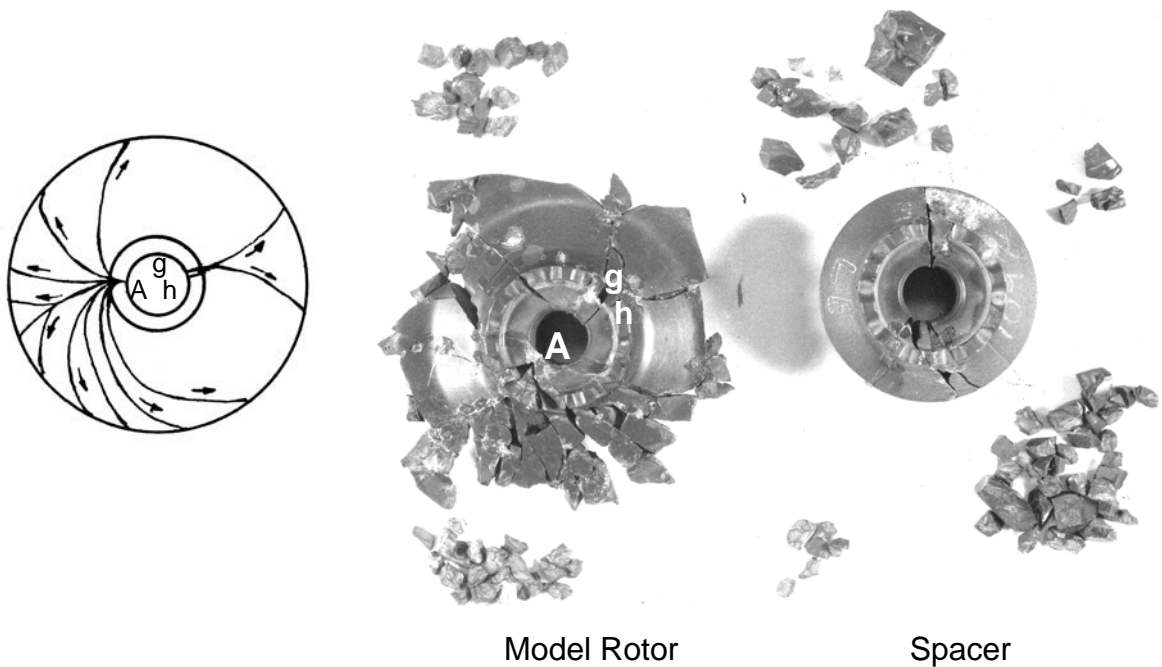


Figure 7 Reconstructed model rotor and spacer. Fracture initiated either at location A on the left side of the bore of the rotor or at two locations g or h on the opposite side of the bore. The schematic on the left shows the radiating pattern on cracks in the rotor.

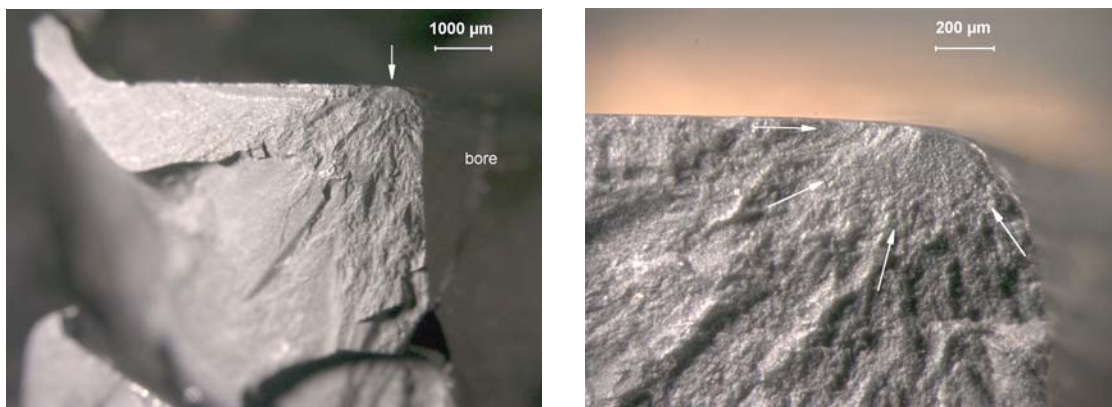


Figure 8 Fracture surfaces showing a fracture mirror and the origin site A, which is a surface crack from grinding. The right figure highlights the fracture mirror with arrows.

CASE 2 The Ceramic Gun Barrel

The U. S. Army has off and on over the past twenty-five years investigated ceramic liners to improve gun barrel life and reduce mass. The low density, high compression strength, refractoriness, and erosion and wear resistance of ceramics could be used to advantage. Figures 9 and 10 show drawings for a 50-caliber machine gun breech with a ceramic liner from a project conducted for the U. S. Army in the 1980's.[18] One design placed the ceramic into compression residual stresses by shrink fitting a steel sleeve around the ceramic. The steel sleeve was heated and placed over the cool ceramic tube. As the assembly cooled, the steel contracted and put the ceramic into radial and hoop compression. The dimensions and temperature differentials were chosen so that the residual axial compression stresses were up to 170 MPa (25 ksi), the radial stresses up to 345 MPa (50 ksi), and the hoop tensile stresses up to 1034 MPa (150 ksi). These were sufficiently high to keep all portions of the ceramic tube in compression when firing stresses were superimposed. The environment is severe and dynamic, but if the ceramic were always under compression, perhaps it would not fracture. Several ceramics were tried, but most testing was on a sintered α -SiC.

So in this case, the designer saw a part that was fully constrained by compression residual shrink fit stresses. After testing, what did the fractographer see?

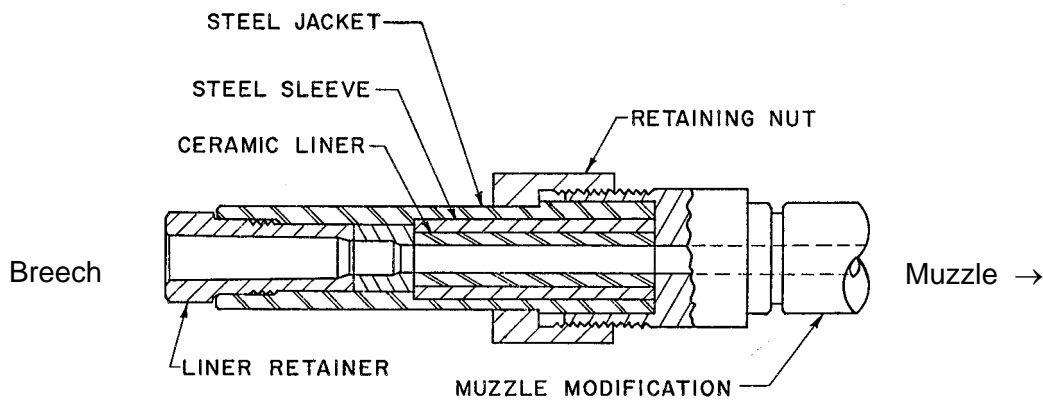


Figure 9 Schematic of the breech end of the 50 caliber (12.7 mm) gun barrel (Adapted from Ref. 18).

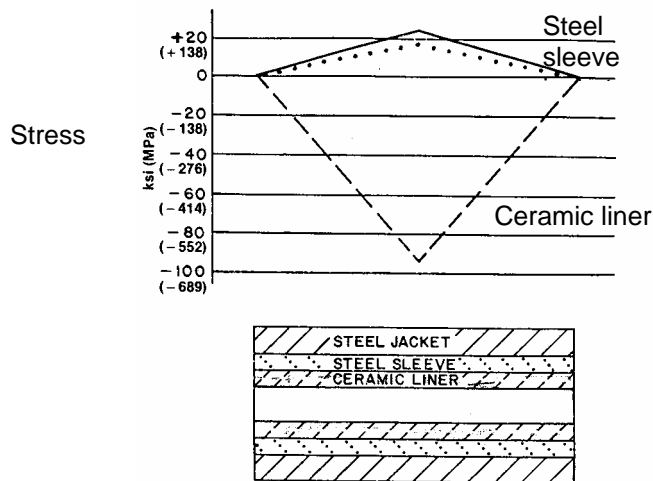


Figure 10 Axial stress distribution in the ceramic inner liner after shrink fitting. (Adapted from Ref. 18).

Some assemblies survived as many as a thousand single shot firings, confounding some skeptics who felt that the assembly would not survive one shot.[18] One assembly that did develop ceramic cracking after a few hundred shots had circumferential fractures as shown in Figure 11a. The steel sleeve and jacket were machined away to allow extraction of the ceramic as shown in Figure 11b. The fracture planes were perpendicular to the axial direction, suggesting that expansion-burst stresses were not the cause of failure, since the latter would have created radial cracking. Fractographic analyses showed that every fragment fractured from one or more contact cracks that were periodically spaced on the *outer rim* of the ceramic.

So if the shrink fitting created compression stresses, where did the tensile stresses come from? The plane of the fractured surfaces and also of the initial semielliptical contact cracks informs us the tensile stresses were axial. Figure 10 shows the axial residual compression stresses did taper off towards the tube ends. The most likely sources of tensile stresses are dynamic stress waves generated during firing. Even if these are initially compressive, they can change phase and become tensile as the stress wave reflects off end faces. Furthermore, the sound velocity and impedance of the silicon carbide and the steel sleeve are not matched and stress waves will propagate at different rates in the axial direction.

The contact stress cracks often were periodic around the rim. Although the parts were machined to tight tolerances, it is likely that slight variations in the mating surfaces led to uneven fit, and hence stress concentration sites that triggered the contact cracks.

So in this case, the ceramic was designed to always be in compression, but fractography showed otherwise. Some design and modeling improvements were suggested. The tolerances and surface specifications for the mating parts could be changed. The elastic properties of the ceramic and the confining sleeve could be matched better. More sophisticated stress models could examine the transient stress states in the assembly.

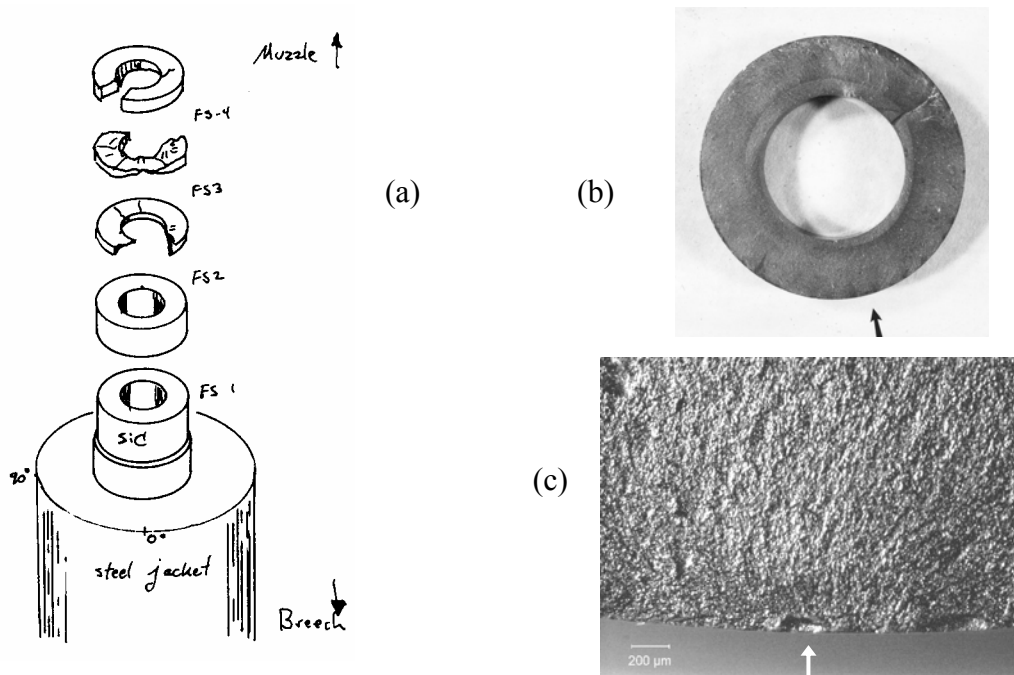


Figure 11 Fractured α -SiC gun barrel (a) is a schematic. (b) shows one fracture surface of one of the ring shaped fragments. The bore diameter is 12.7 mm. The arrow shows a contact crack origin on the outer surface where it contacted the steel sleeve. A close-up is shown in (c).

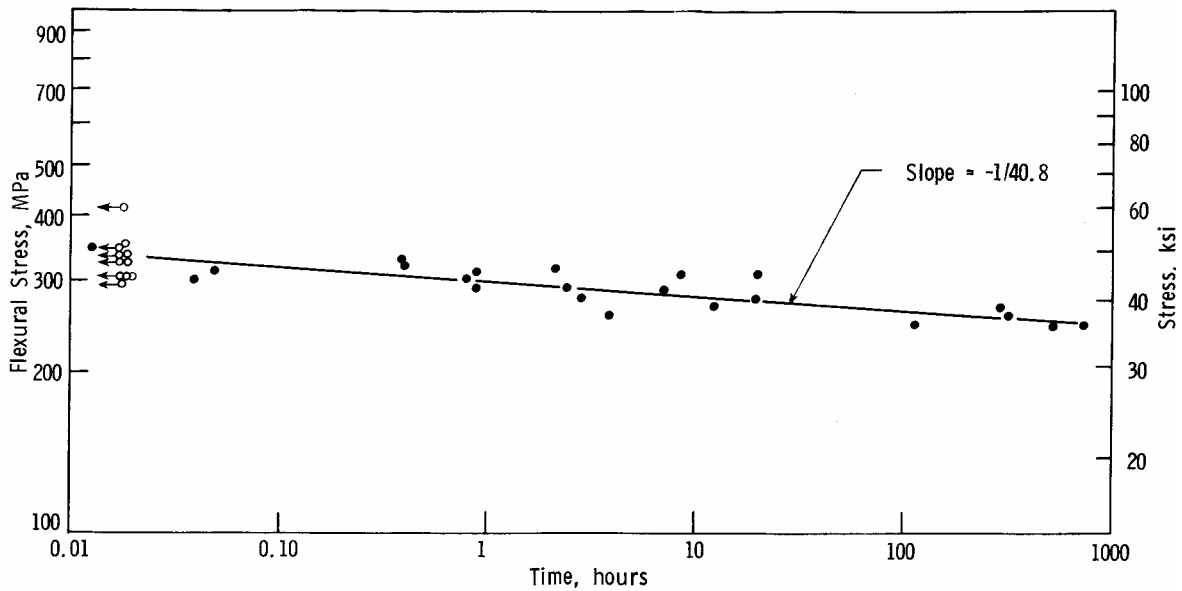


Figure 12 Stress rupture curve at 1200 °C in air for sintered α -SiC [19-21] Every time dependent fracture was from a pore or porous zone, and only if it was surface connected.

CASE 3 Conflicting Stress Rupture Data for Sintered α Silicon Carbide

This case is not about a specific component, but about the risk of treating all flaws as if they behave the same. As part of a program on characterization of structural ceramics for heat engine ceramics in the 1980's, the author conducted extensive stress rupture testing of] including pressureless sintered α -SiC.^c [19,20,21 At elevated temperatures, there was a distinct trend of time dependent failure for bend bars tested in air such as shown in Figure 12. Trend like this are usually interpreted as evidence of slow crack growth. Tests of two other batches made in different years confirmed that time dependent failure always occurred at 1200 °C and above. On the other hand, another team [22] had data that matched the ≥ 1300 °C data, but contradicted the 1200 °C data. They did not observe any time dependent fractures at 1200 °C. Why did the two groups have such contrasting outcomes at 1200 °C?

Fractographic analysis provided the answer.[19-21] At 1300 °C and above, easily detected intergranular slow crack growth from volume-distributed flaws such as large grains, pores, or agglomerates caused fracture such as shown in Figure 13a. Some of these volume origins were located in the bulk. Both teams detected this behavior.

A different story emerged at 1200 °C. Every one of the time-dependent fracture origins in references 19-21 was a pore or porous region and every one was connected to the outer surface as shown in Figure 13b. These flaws not have slow crack growth markings. Evidently the pore type flaws were susceptible to very localized stress corrosion cracking (from oxidation) that sharpened or locally extended tiny microcracks on the pore periphery. Not much change in flaw size or severity was necessary for these flaws to go critical, since they broke at stresses very close to the fast fracture strength as shown in Figure 12.

The other testing team did not detect this stress corrosion mechanism since they used Knoop artificial flaws in all of their bend specimens.[22] Artificial flaws often are effective tools for studying fracture, but in this instance they produced misleading results. The Knoop

^c Hexoloy SA, Carborundum, Niagara Falls, NY.

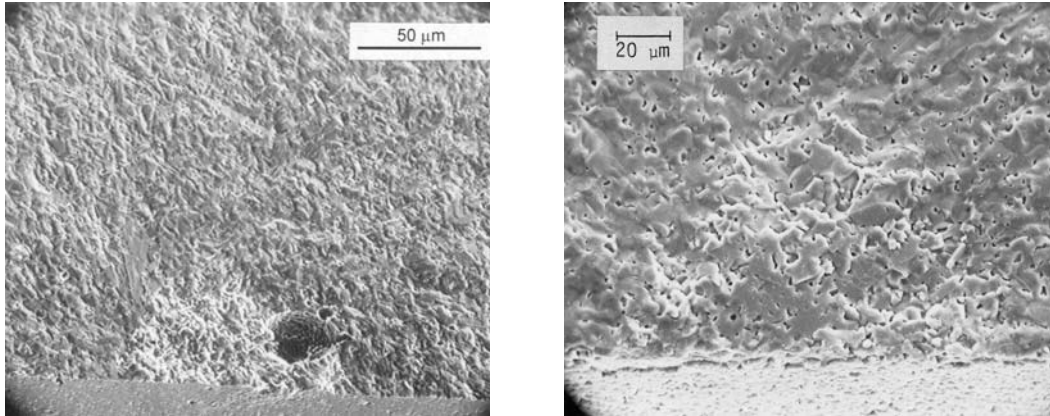


Figure 13. Fracture origins in stress rupture specimens. (a) shows a classic slow crack growth zone in a specimen that broke at 1300 °C. (b) shows a surface connected porous zone in a specimen that broke at 863 hours at 1200 °C.

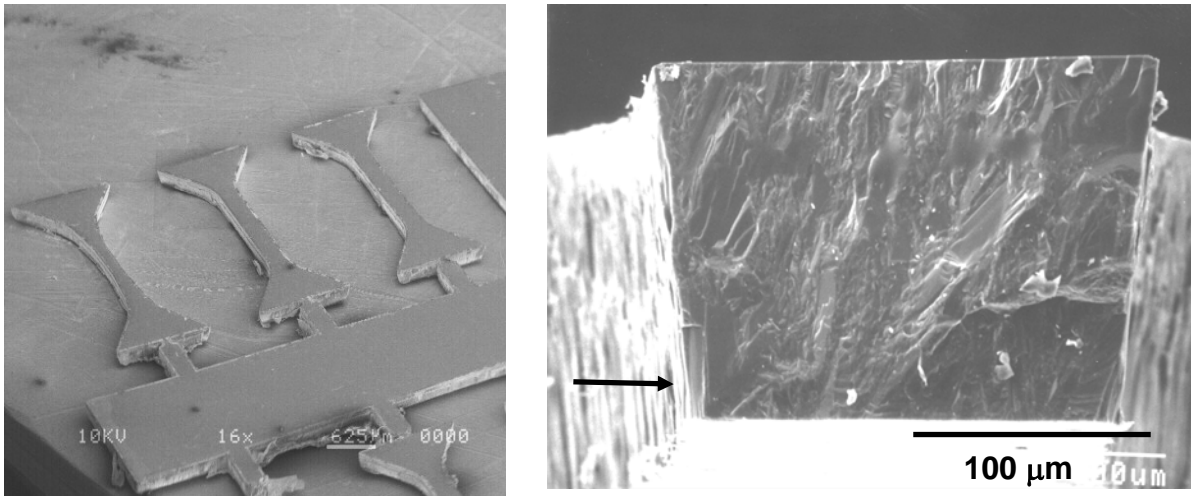
flaws did grow by slow crack growth at 1300 °C and above. The Knoop flaws did not grow by slow crack growth or by stress corrosion at 1200 °C. One might ask why the specimens with Knoop flaws did not fracture from the pores and porous regions that were undoubtedly present. The answer is that the Knoop flaws reduced the strength of the specimens to less than 200 MPa, a stress well below that necessary to activate the pore flaw stress corrosion mechanism.

In summary, three flaws types controlled the room temperature strength as well as acted as sources of time dependent fracture at 1300 °C: pores and porous regions, large grains, and agglomerates. Only pores and porous zones were vulnerable to time dependent stress corrosion cracking at 1200 °C, and *only* if they were connected to the surface. A reliability model that assumed no time dependent failure at 1200 °C in air would have been faulty. This case demonstrates that it is often best to let a material reveal what type of flaws it is apt to fail from.

CASE 4 Strength Data for Miniature Silicon Carbide Tensile Specimens

Testing methodologies must keep pace with emerging technologies for miniature devices and structures for microelectromechanical systems (MEMS) and even smaller devices. Sharpe et al. [23] recently investigated the strength of miniature silicon carbide specimens with cross section sizes of $\approx 200 \mu\text{m}$ or less prepared by chemical vapor deposition (CVD) followed by deep reactive ion etching to final shape. Specimens with three types of gage section were used as shown in Figure 14. The curved gage section specimens were prepared to eliminate a stress concentration at the end tab - gage section junction, and consequently had narrower gage sections. The curved specimens had a good distribution of breakages in the gage section, unlike the straight specimens which sometimes broke at the end of the gage section. Consequently the curved gage section specimens were used as the baseline data set. Weibull statistics were applied to scale the strengths and to determine whether surface or volume flaw scaling gave better correlation.

Fractographic analysis was difficult but productive. The coarse microstructure created a very rough fracture surface that masked common fracture markings. Large SiC grains affected the crack propagation across the fracture surface, causing significant crack redirection and severe roughness as the propagating crack sought out preferred cleavage planes. The most helpful features for pinpointing the origin were twist hackle lines on cleaved grains and occasional large



(a)

(b)

Figure 14 (a) shows the miniature 3.1 mm long SiC tensile specimens. From the left: curved, straight and small notched gage sections. The notches are too small to be seen in this view. (b) shows the fracture surface of a straight section specimen. The arrow shows the origin is a $25\ \mu\text{m} \times 50\ \mu\text{m}$ large grain at the root of an etch groove. (Ref. 23)

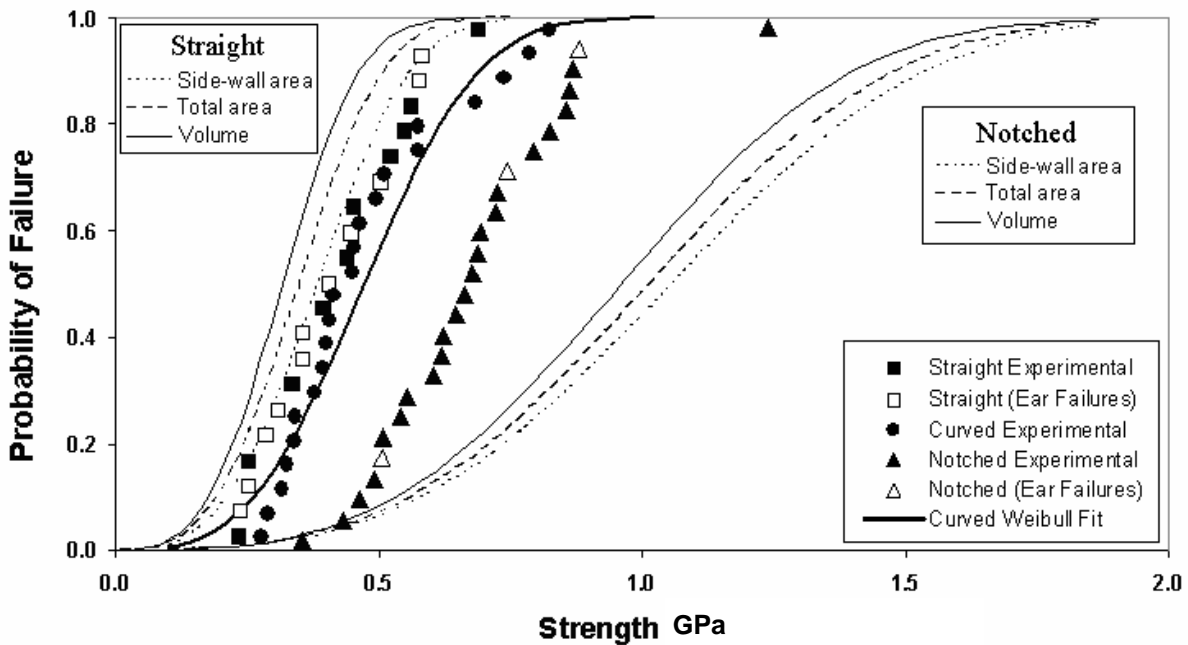


Figure 15 Strength distributions for straight, curved, and notched specimens. Using the curved specimen data set as the baseline, the straight specimen strengths agreed with the Weibull scaling prediction if sidewall area scaling was used. Correlations were poor for notched specimens.[23]

hackle lines that showed the local direction of crack propagation. This enabled the observer to backtrack to the origin site.

Figure 15 shows the strength results for the straight, curved, and notched specimens. The Weibull moduli were quite low (3 to 4) and the standard deviations quite large attesting to significant material or flaw variability. The fracture origins in all three specimen types usually were a combination of a deep etch groove that combined with a large columnar grain with a favorable orientation so that a crack could pop in on a preferred cleavage plane. Thus, the critical flaws were in many cases a combination of the sidewall grooves and a large grain: a hybrid surface-volume type flaw.

Nevertheless, the fractographic results supported the Weibull area scaling for comparing the straight and curved specimens, provided that only the etched *sidewall* areas were used. Weibull scaling to predict the notched specimen strengths was not successful and fractography provided an explanation. The notches were quite small (15 μm to 25 μm radius) and not much larger than some of the grains and the notch itself. Hence, a Weibull analysis based on continuum mechanics is questionable.

CONCLUSIONS

Ceramics are unforgiving materials when loaded in tension. The track record of reliability analysis of structural ceramics is mixed in large part due to the many assumptions implicit in the reliability analysis. Violation of any one of these “weakest links” incurs considerable risk. Nevertheless, there are a number of very successful applications, some of which are cataloged in the review paper by Quinn and Morrell.[11] Judicious fractographic analysis of both laboratory strength coupons and destructive prototype test coupons can dramatically improve models. It is best to let the material reveal how it is apt to fail than rigidly adhere to a preconceived model.

ACKNOWLEDGEMENT

Support for this work was furnished by the U. S. Department of Energy, Office of Transportation Technologies, with Oak Ridge National Laboratory.

REFERENCES

- ¹ W. Weibull, “A Statistical Distribution Function of Wide Applicability,” *J. Appl. Mech.*, **18**, 293–297 (1951).
- ² R. W. Davidge, *Mechanical Behavior of Ceramics*, Cambridge Univ. Press, London, 1979.
- ³ D. Munz and T. Fett, *Ceramics, Mechanical Properties, Failure Behavior, Materials Selection*, Springer, Berlin, 1999.
- ⁴ W. E. C. Creyke, I. E. J. Sainsbury, and R. Morrell, *Design with Non-ductile Materials*, Applied Science Publ., London, 1982.
- ⁵ J. B. Wachtman, *Mechanical Properties of Ceramics*, Wiley, New York, 1996.
- ⁶ *Life Prediction Methodologies and Data for Ceramic Materials*, ASTM Special Technical Publication 1201, eds, C. R. Brinkman and S. F. Duffy, ASTM, West Conshohocken, PA, 1994.
- ⁷ J. Menčík, *Strength and Fracture of Glass and Ceramics*, Elsevier, Amsterdam, 1992.
- ⁸ A. Paluszny and W. Wu, “Probabilistic Aspects of Designing with Ceramics,” ASME paper 77-GT-41 (1977).
- ⁹ A. De S. Jayatilaka, *Fracture of Engineering Brittle Materials*, Applied Science Publ., London, 1979.

-
- ¹⁰ R. Morrell, "Mechanical Properties of Engineering Ceramics: Test Bars Versus Components," *Mat. Sci. and Eng.*, **A109**, 131–137 (1989).
- ¹¹ G. D. Quinn and R. Morrell, "Design Data for Engineering Ceramics: A Review of the Flexure Test," *J. Am. Ceram. Soc.*, **74**, [9] 2037–2066 (1991).
- ¹² R. R. Baker, L. R. Swank, and J. C. Caverly, "Ceramic Life Prediction Methodology - Hot Spin Disk Life Program," AMMRC TR 83-44, Army Materials and Mechanics Research Center, Watertown, MA, August, 1983.
- ¹³ L. R. Swank, R. R. Baker, and E. M. Lenoe, "Ceramic Life Prediction Methodology," pp. 323–330 in Proceedings of the 21st Automotive Technology Development Contractors Coordination Meeting, Society of Automotive Engineers, Warrendale, PA, 1984.
- ¹⁴ G. D. Quinn, K. Xu, R. J. Gettings, J. A. Salem, and J. J. Swab, "Does Anyone Know the Real Fracture Toughness? SRM 2100: The World's First Ceramic Fracture Toughness Reference Material," pp. 76-93 in *Fracture Resistance Testing of Monolithic and Composite Brittle Materials*, ASTM STP 1409, J. A. Salem, G. D. Quinn, and M. G. Jenkins, eds. ASTM, West Conshohocken, PA, 2002.
- ¹⁵ G. D. Quinn, "Fracture Mechanism Maps for Advanced Structural Ceramics, Part I, Methodology and Hot Pressed Silicon Nitride," *J. Mat. Sci.*, **25**, 4361-76 (1990).
- ¹⁶ G. D. Quinn and J. B. Quinn, "Slow Crack Growth in Hot Pressed Silicon Nitride," pp. 603 – 636 in *Fracture Mechanics of Ceramics 6*, Eds. R. Bradt, A. Evans, D. Hasselman, F. Lange, Plenum Press, NY, (1983).
- ¹⁷ K. D. Mörgenthaler and E. Tiefenbacher, "Bauteile Aus Keramik Für Gasturbinen," (Ceramic Components for Gas Turbines), Final Report of Phase III, Daimler-Benz AG, Technical Report, Stuttgart, 1983.
- ¹⁸ E. J. Bunning, D. R. Claxton, and R. A. Giles, "Liners for Gun Tubes – A Feasibility Study," *Ceram. Eng. and Sci. Proc.*, 2 [7-8] 509–519 (1981).
- ¹⁹ G. D. Quinn, "Characterization of Turbine Ceramics After Long Term Environmental Exposure," AMMRC TR 80-15, Army Materials and Mechanics Research Center, Watertown, MA, May 1980.
- ²⁰ G. D. Quinn, "Review of Static Fatigue in Silicon Nitride and Silicon Carbide," *Ceram. Eng. and Sci. Proc.*, **3**, [1-2] 77– 98 (1982).
- ²¹ G. D. Quinn and R. N. Katz, "Time Dependent High Temperature Strength of Sintered Alpha SiC," *J. Amer. Ceram. Soc.*, **63**, [1-2] 117– 119 (1980).
- ²² J. Coppola, M. Srinivasan, K. Faber, and R. Smoak, "High Temperature Properties of Sintered Alpha Silicon Carbide," presented at *the International Symposium on Factors in Densification and Sintering of Oxide and Non-Oxide Ceramics*, Hakone, Japan, October 1978.
- ²³ W.N. Sharpe, Jr., O. Jadaan, G.M. Beheim, G.D. Quinn, N.N. Nemeth, "Fracture Strength of Silicon Carbide Microspecimens," accept by *J. Micromechanical Systems*, 2004.